PHYS722/822

From Particle to Nuclear Physics

Sebastian Kuhn

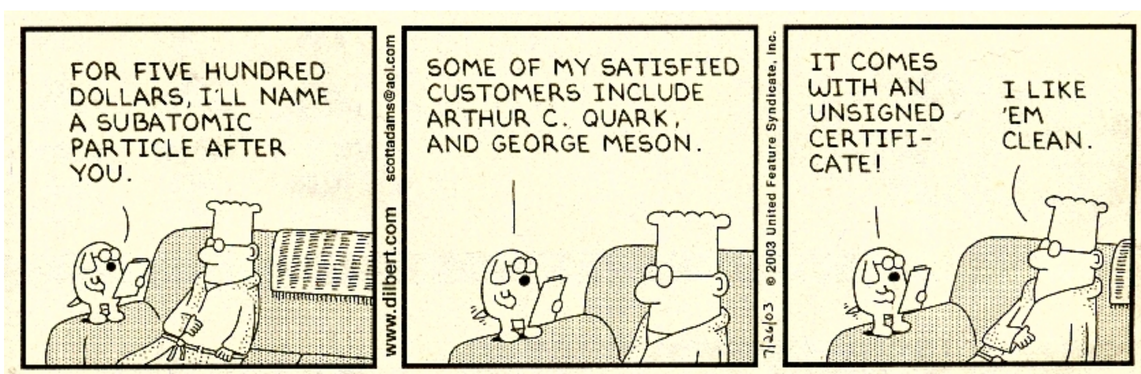

Hadron Structure

- Simple-most (constituent quark) model of nucleons (protons and neutrons)
- … becomes much more complicated once we consider the full relativistic quantum field theory called QCD

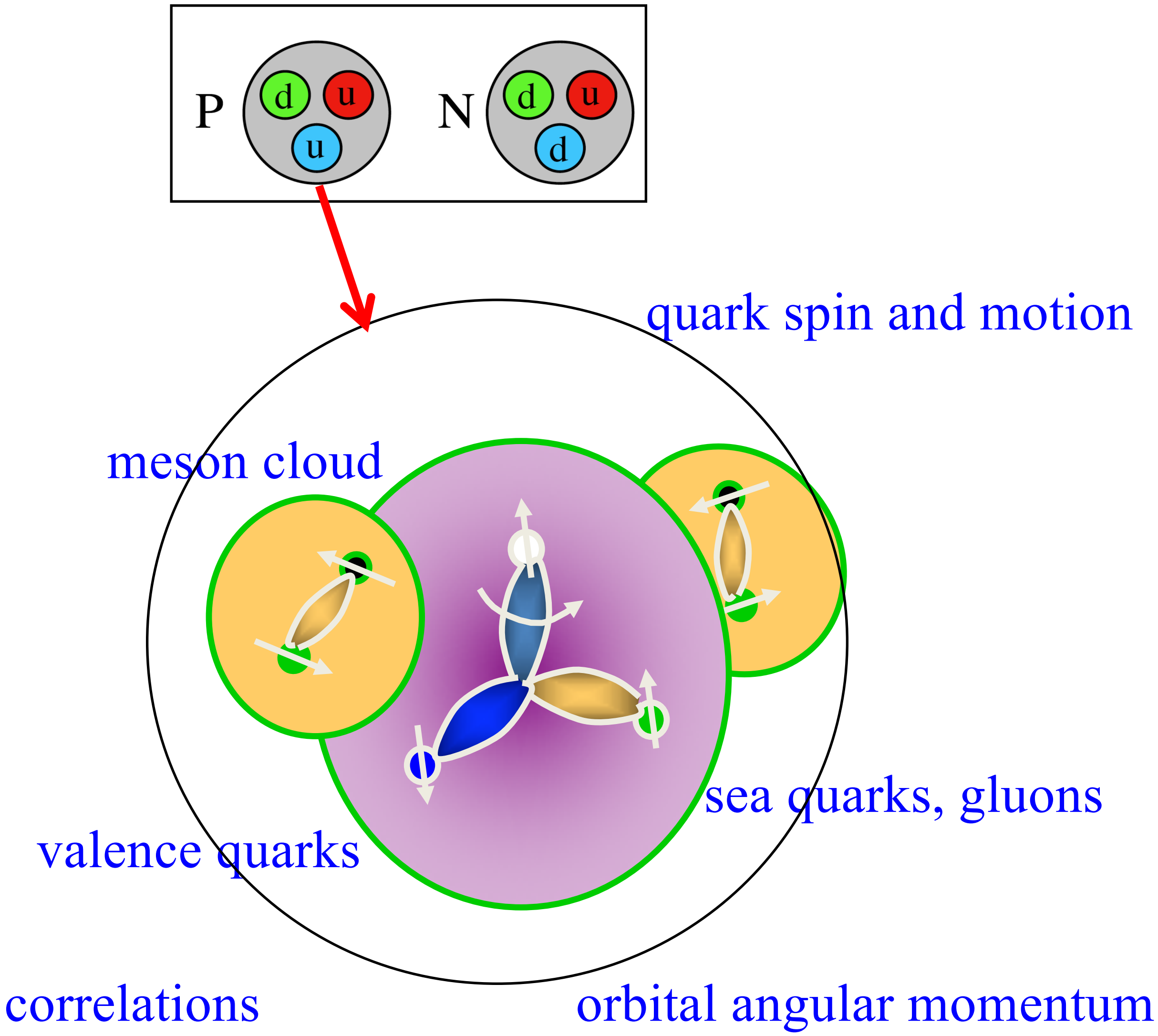

QCD = Quantum Chromo Dynamics = theory of strong interactions between quarks and gluons

Nuclear Structure

- Even more complicated!

- Nuclei effectively look like a bunch of nucleons, mesons, nucleon resonances… bound together by the strong interaction

- Ultimately, must be explained in terms of quarks and gluons, as well!

- Quark structure might be modified (EMC effect) and in turn affects nuclear binding

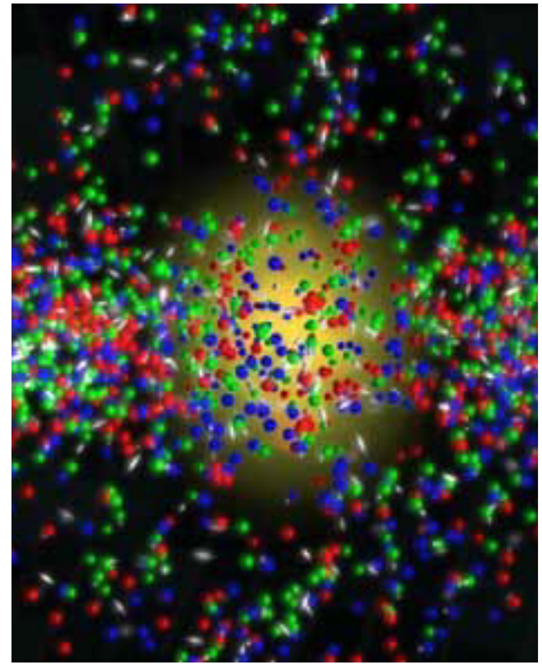

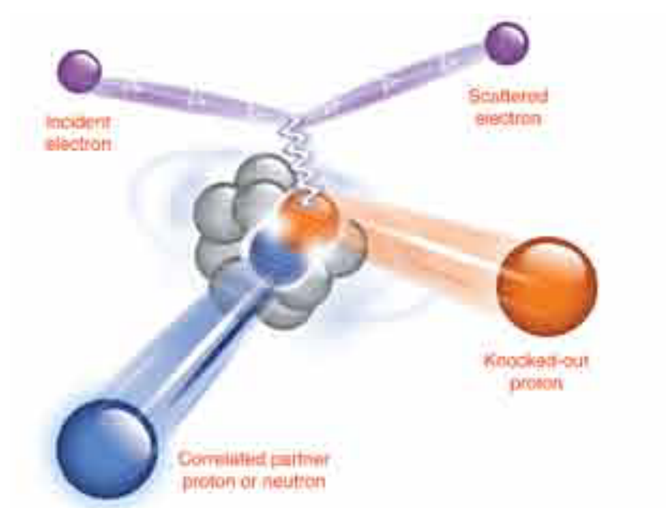

NN scattering

- Basic scattering theory
  - Asymptotic states
  - Plane wave plus spherical outgoing wave
  - Current densities
- Observables
  - Cross section
  - Polarization observables

Example of NN data used in PSA

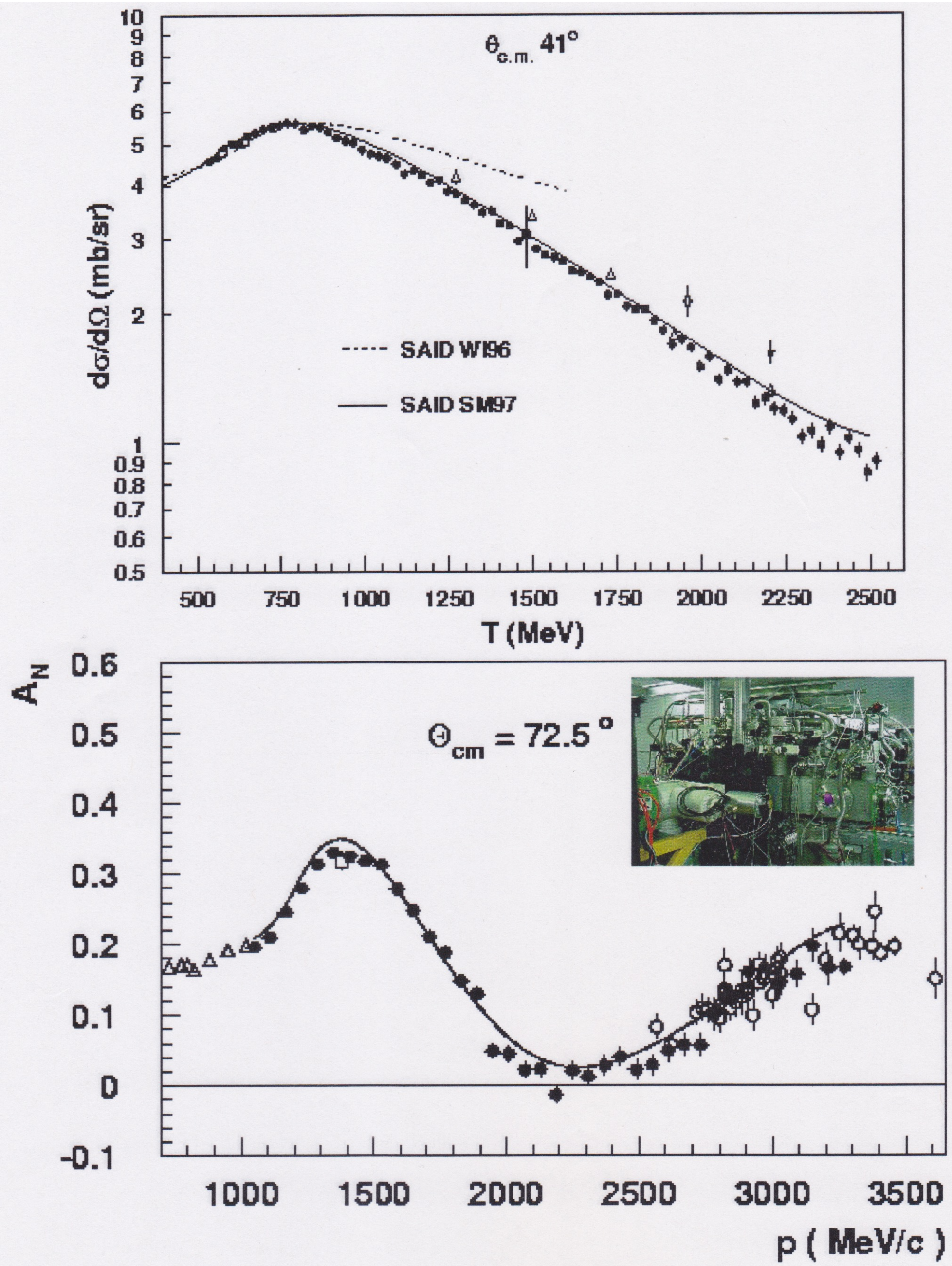

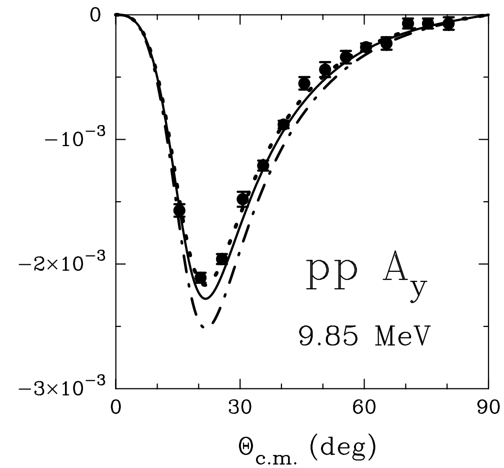

Figure 8. The proton-proton analyzing power A_y at 9.85 MeV. The theoretical curves are calculated with $g^2_{\pi^0}/4\pi = 13.2$ (dotted), 13.6 (solid, Model A), and 14.4 (dash-dot, Model D) and fit the data with a χ^2/datum of 0.98, 2.02, and 9.05, respectively. The solid dots represent the data taken at Wisconsin [73].

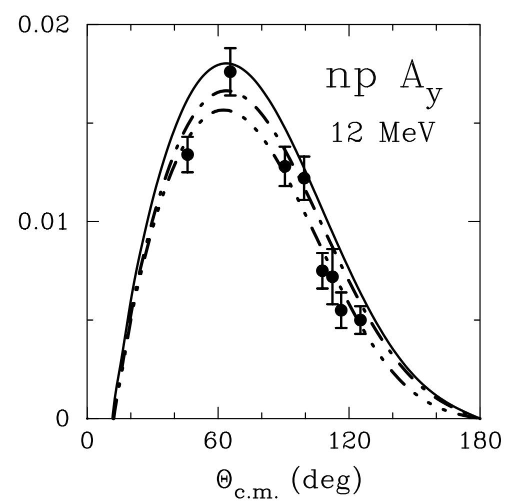

Figure 9. The neutron-proton analyzing power A_y at 12 MeV. The theoretical curves are calculated with $g^2_{\pi^0}/4\pi = g^2_{\pi^\pm}/4\pi = 13.6$ (solid line, Model A), $g^2_{\pi^0}/4\pi = g^2_{\pi^\pm}/4\pi = 14.4$ (dash-dot, Model D), and the charge-splitting $g^2_{\pi^0}/4\pi = 13.6$, $g^2_{\pi^\pm}/4\pi = 14.4$ (dash-3dot, Model E). The solid dots represent the data taken at TUNL [74].

NN Scattering – a Reminder

what can we measure?

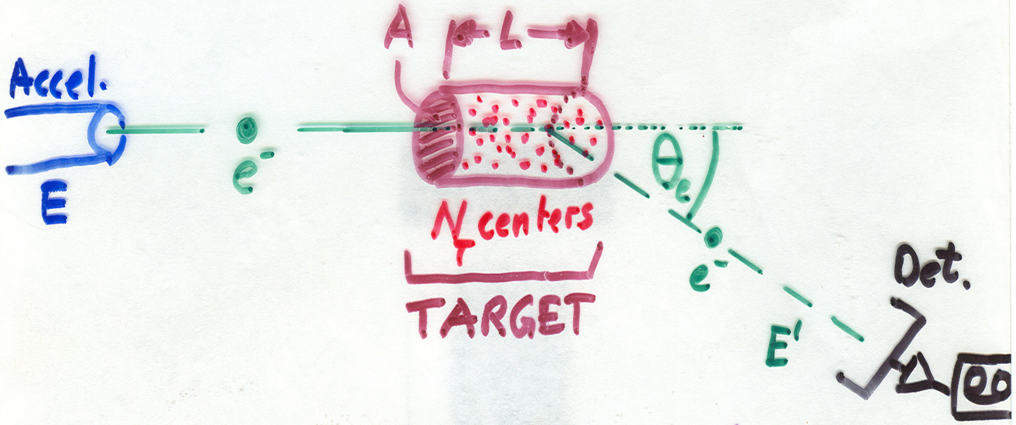

What is the likelihood to find the electron scattered into the detector?

$$P \sim n_T \cdot L = \frac{N_T}{A\,L} \cdot L = \frac{N_T}{A}\ ^{*}$$

$$\Rightarrow \text{ call } \quad \Delta\sigma = P / \left(\frac{N_T}{A}\right) \quad \text{(cross section)}$$

$\Delta\sigma$ <u>DEPENDS</u> on the kinematics (E, E', θ_e) and is $\approx$ proportional to <u>SIZE</u> of kinematic bin spanned by the detector

*Note: $\frac{N_T}{A} = \rho\left[\frac{g}{cm^3}\right] \cdot L\,[cm] \cdot \frac{\text{Avogadro}}{\text{Atomic Weight [u]}}$

Theorist's View

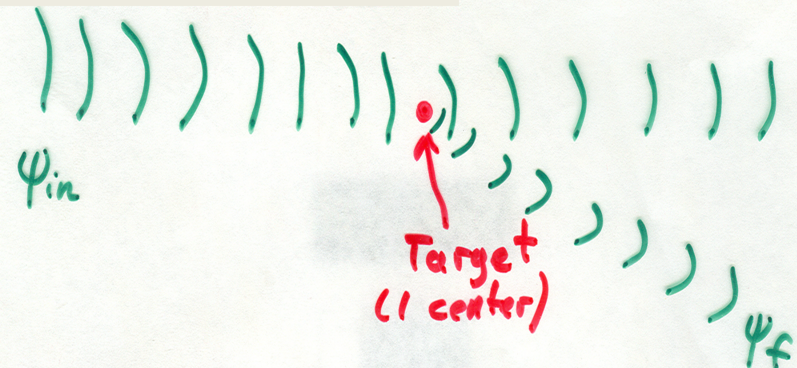

What is the transition rate $W_{i\to f}$?

$$\dot{N}_{e,f} = \dot{N}_{e,in} \cdot P(i\to f) = I_{e,in} \cdot \frac{N_T}{A} \cdot \Delta\sigma$$

$$= \frac{I_{e,in}}{A} \cdot N_T \cdot \Delta\sigma = \left|\vec{j}_{e,in}\right|_2 \cdot N_T \cdot \Delta\sigma$$

$$\Rightarrow W_{i\to f} = j_{in} \cdot \Delta\sigma$$

Fermi's GOLDEN Rule:

$$W_{i\to f} = \frac{2\pi}{\hbar} \left|\mathcal{M}_{fi}\right|^2 \Delta\phi$$

Phase space spanned by detector / kinematic bin

$$\mathcal{M}_{fi} = \langle \psi_f \,|\, H_{int} \,|\, \psi_{in} \rangle$$

NN scattering

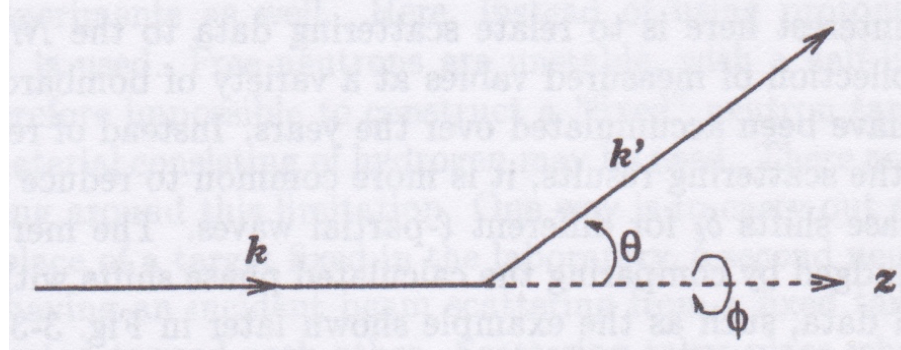

- Basic scattering theory
  - Solve Schrödinger Equation: $-\frac{\hbar^2}{2\mu}\nabla^2\psi + (V-E)\psi = 0$
  - Asymptotic free states: Plane wave plus spherical outgoing wave $\psi(r,\theta,\phi) \xrightarrow[r\to\infty]{} e^{ikz} + f(\theta,\phi)\frac{e^{ikr}}{r}$
  - Current densities

$$S(r,t) = \frac{\hbar}{2i\mu}\{\psi^*\nabla\psi - \psi\nabla\psi^*\} = \Re\left\{\psi^*\frac{\hbar}{i\mu}\nabla\psi\right\} = \Re\left\{e^{-ikz}\frac{\hbar}{i\mu}\frac{d}{dz}e^{ikz}\right\} = \frac{\hbar k}{\mu} = v$$

$$S_r = \Re\left\{\left(f(\theta)\frac{e^{ikr}}{r}\right)^*\frac{\hbar}{i\mu}\frac{d}{dr}\left(f(\theta)\frac{e^{ikr}}{r}\right)\right\} = \frac{v}{r^2}|f(\theta)|^2 + O(r^{-3})$$ See HW 8

  - Cross section

$$d\Omega = \frac{da}{r^2} \qquad N_r = S_r\,da = S_r r^2\,d\Omega \qquad \frac{d\sigma}{d\Omega} = \frac{S_r r^2}{S_i} = |f(\theta)|^2$$

Potential Scattering

- Angular momentum decomposition

$$\psi(r,\theta) = \sum_{\ell=0}^{\infty} a_\ell Y_{\ell 0}(\theta)\, R_\ell(k,r)$$

$$R_\ell(k,r) \xrightarrow{\text{free}} j_\ell(kr) \xrightarrow[r\to\infty]{\text{free}} \frac{1}{kr}\sin(kr - \tfrac{1}{2}\ell\pi) \xrightarrow[r\to\infty]{\text{scatt.}} \frac{1}{kr}\sin(kr - \tfrac{1}{2}\ell\pi + \delta_\ell)$$

- Phase shifts -> scattering amplitude ->cross section

$$f(\theta) = \frac{\sqrt{4\pi}}{k}\sum_{\ell=o}^{\infty}\sqrt{2\ell+1}\, e^{\imath\delta_\ell}\sin\delta_\ell Y_{\ell 0}(\theta)$$

Phase Shifts – Example square potential scattering

$$\kappa = \frac{1}{\hbar}\sqrt{2\mu(E+V_0)} \qquad u_0(r) = \sin(kr+\delta_0) \quad \text{for} \quad r > r_0$$

$$\frac{\sin \kappa r_0}{\kappa \cos \kappa r_0} = \frac{\sin(kr_0+\delta_0)}{k\cos(kr_0+\delta_0)}$$

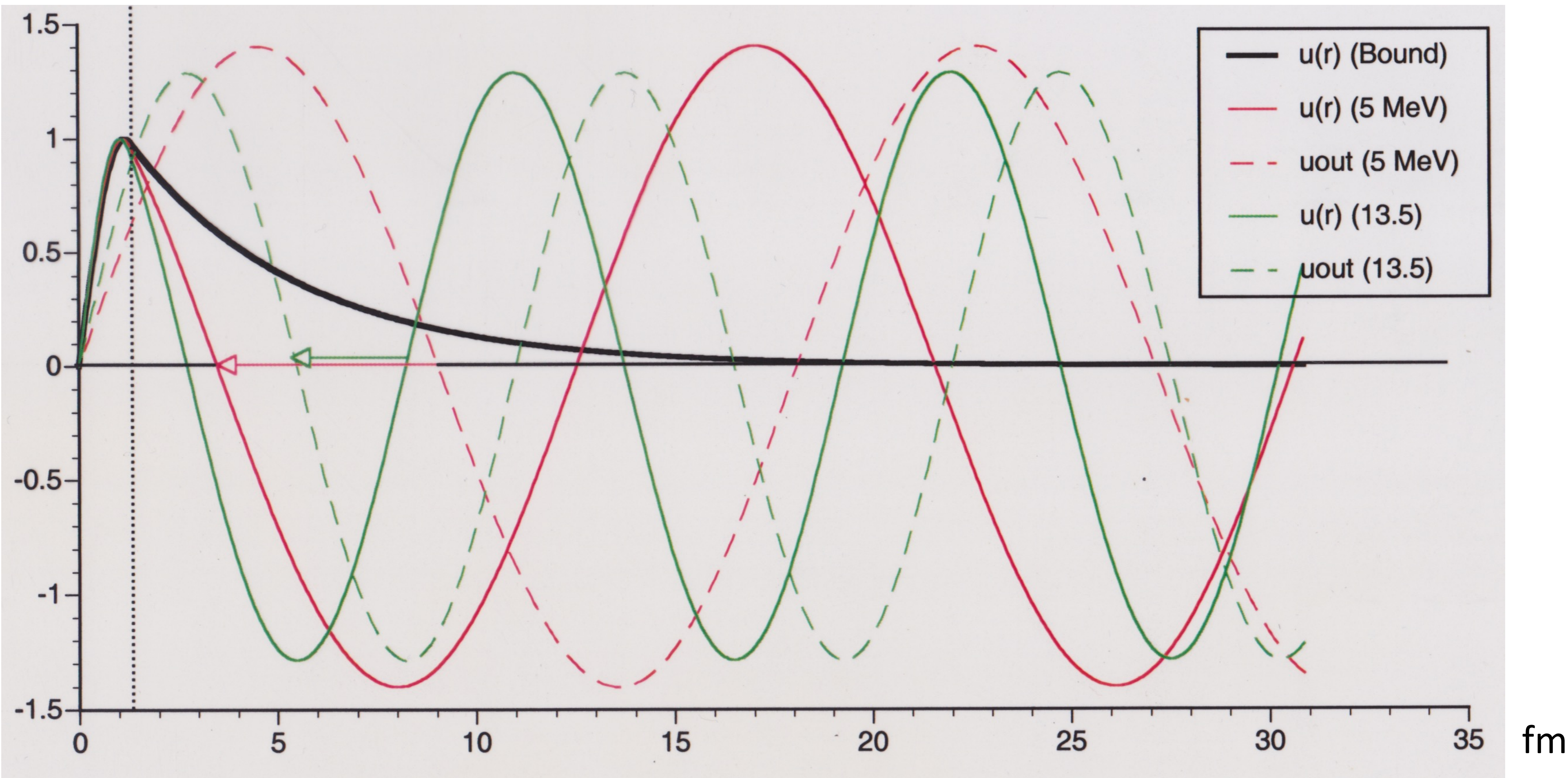

Selection rules for NN phase shifts

- I = 0 (pn only):
  - Isospin WF antisymmetric ->
  - Spin-orbital WF symmetric ->
  - Either S = 1 and L = 0,2,4,…
  - Or S = 0 and L = 1, 3,…
- I = 1 (pp, pn and nn)
  - Either S = 0 and L = 0,2,4,…
  - Or S = 1 and L = 1, 3,…
- Can also have transition Phase shifts!

Nomenclature:

$^{2S+1}L_J$; $\mathbf{J} = \mathbf{L} + \mathbf{S}$

Ex.: $\boxed{^3S_1,\ ^3D_1}$, $^3D_2$, $^3D_3$

Ex.: $^1P_1$, $^1F_3$,

Ex.: $^1S_0$, $^1D_2$,

Ex.: $^3P_0$, $^3P_1$, $^3P_2$, $^3F_2$, $^3F_3$, $^3F_4$

Ex.: $^3S_1 \leftrightarrow {}^3D_1$, $^3P_2 \leftrightarrow {}^3F_2$

NN Phase Shifts

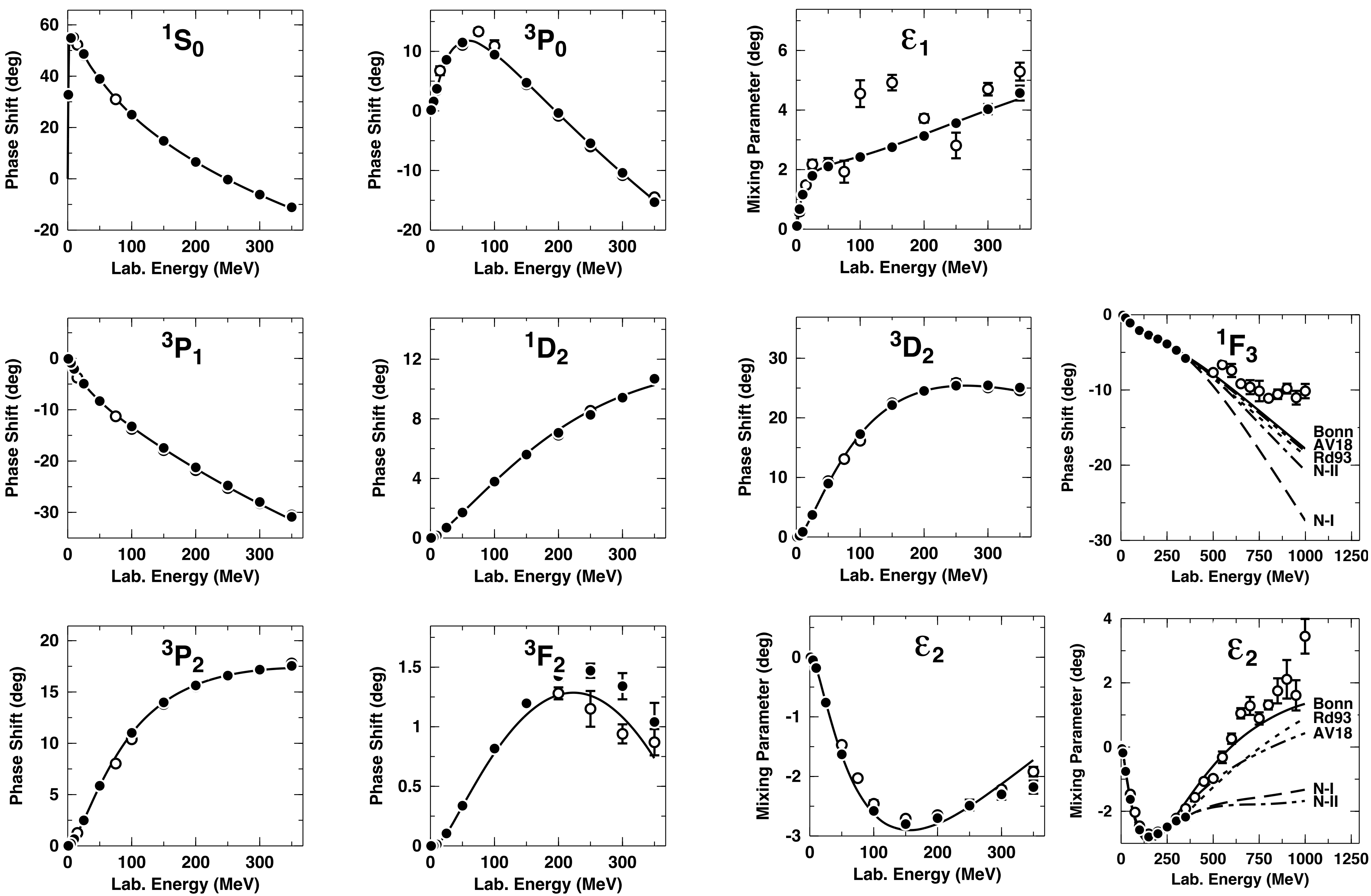

The NN Force

- (L)QCD: The future
- QCD-based effective theories
  - Chiral Perturbation Theory
  - Pion-less effective theory
- Models
  - Quark exchange, gluon van-der Waals force (QCD-"inspired")
  - Meson exchange + hard core
    - Pauli Principle between quarks? Spin-Spin interaction? Vector Mesons?

LQCD

(copied from a Lecture by R. Schiavilla 10/20/2017)

NPLQCD calculations ($m_\pi = 806$ MeV)

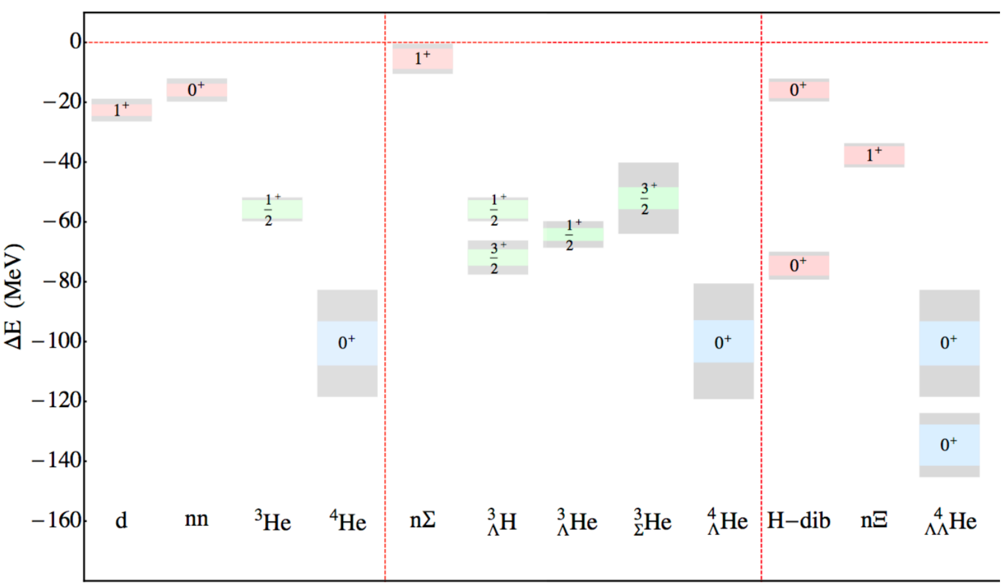

Beane *et al.* (2013)

LQCD calculation of $2N$ potential by HAL collaboration

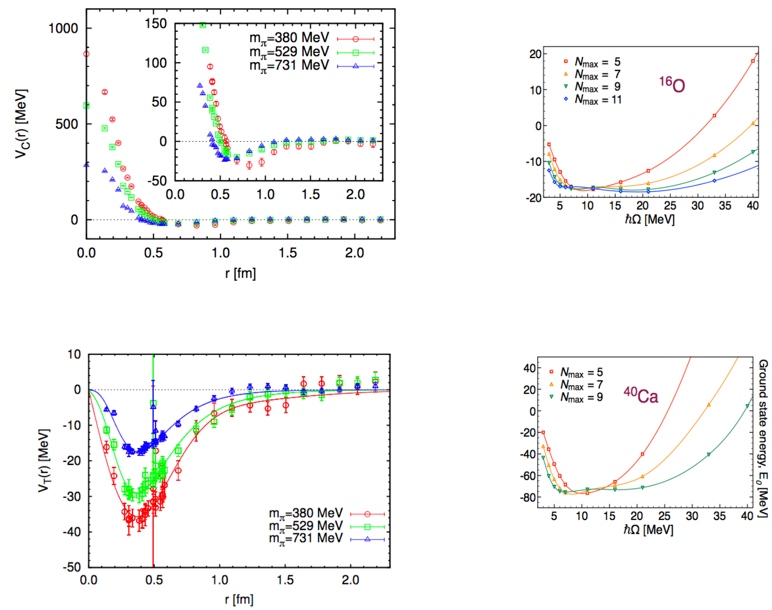

Aoki *et al.* (2012); McIlroy *et al.* (2017)

χPT effective potential

(also from Rocco)

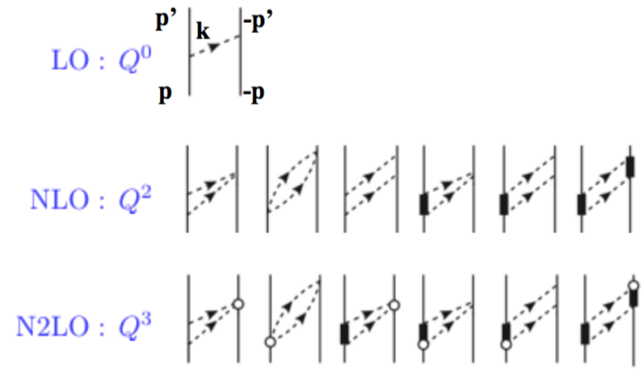

From PHYSICAL REVIEW C **94**, 054007 (2016):

The v_L part includes the one-pion-exchange (OPE) and two-pion-exchange (TPE) (including Deltas) contributions up to N2LO. Short range part "ad hoc".

$$v_{12}^{\mathrm{L}} = \left[\sum_{l=1}^{6} v_{\mathrm{L}}^{l}(r)\, O_{12}^{l}\right] + v_{\mathrm{L}}^{\sigma T}(r)\, O_{12}^{\sigma T} + v_{\mathrm{L}}^{tT}(r)\, O_{12}^{tT},$$

where

$$O_{12}^{l=1,\ldots,6} = [\mathbf{1}\,,\, \boldsymbol{\sigma}_1\cdot\boldsymbol{\sigma}_2\,,\, S_{12}] \otimes [\mathbf{1}\,,\, \boldsymbol{\tau}_1\cdot\boldsymbol{\tau}_2],$$

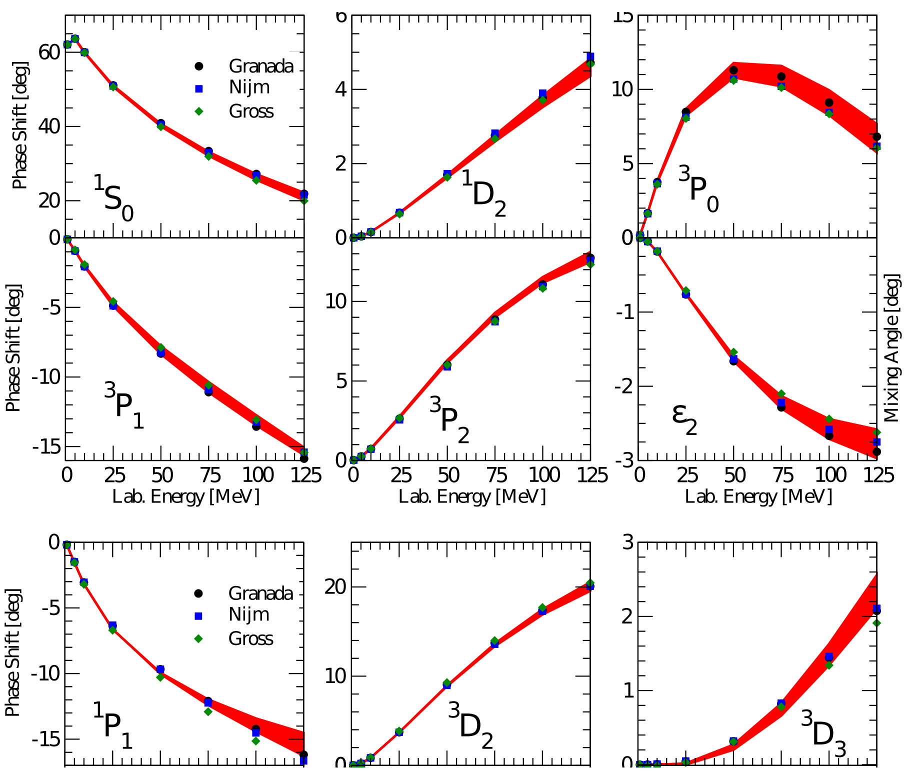

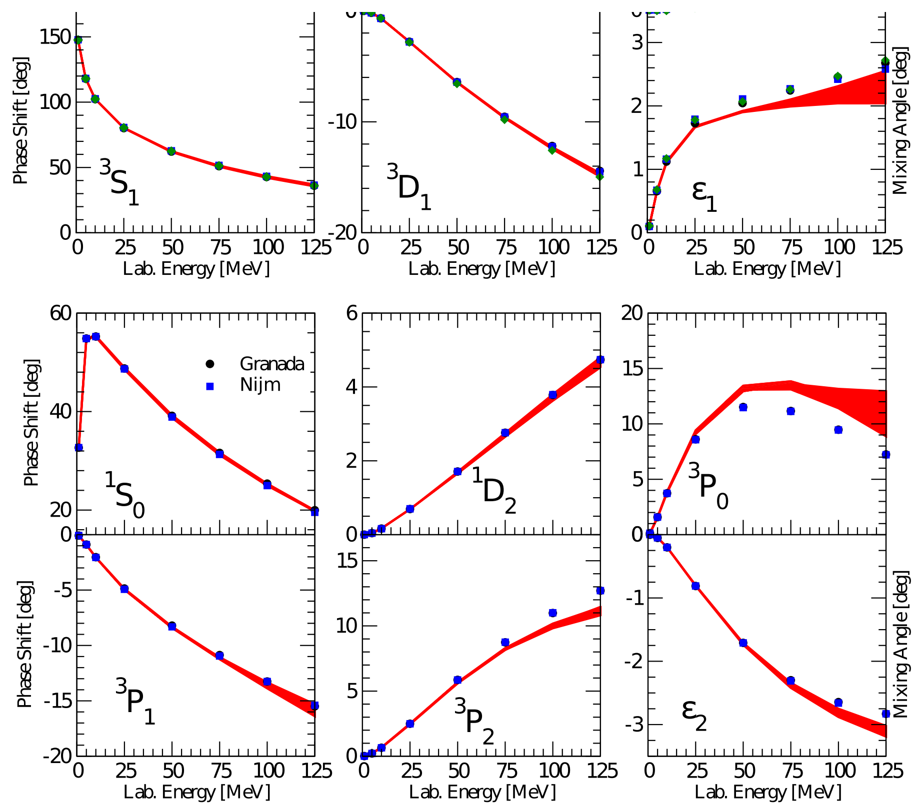

Meson Exchange

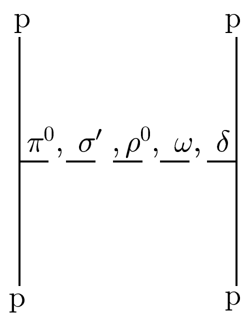

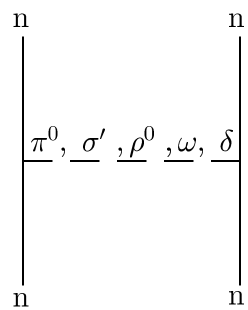

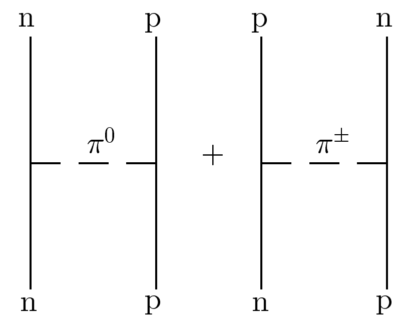

Plus 2-pion ("sigma", rho) exchange plus intermediate nucleon excitations

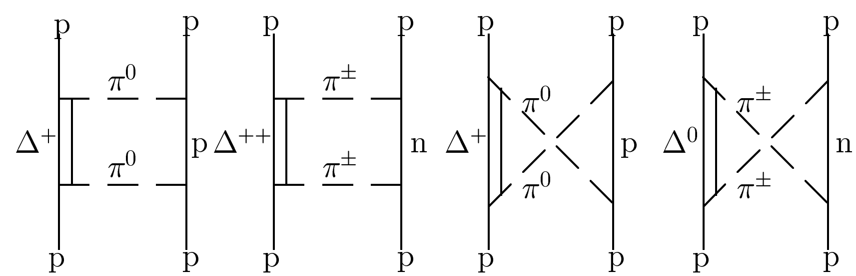

(a)

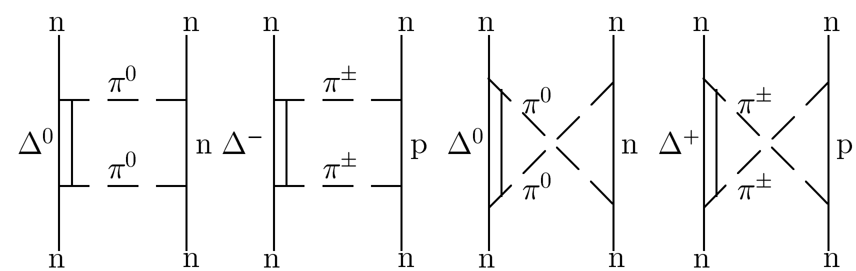

One Pion Exchange (OPE)

(again borrowing from Rocco: Rev. Mod. Phys., Vol. 70, No. 3, July 1998)

$$v_{ij}^{OPE} = \frac{f_{\pi NN}^2}{4\pi}\frac{m_\pi}{3}[Y_\pi(r_{ij})\boldsymbol{\sigma}_i\cdot\boldsymbol{\sigma}_j + T_\pi(r_{ij})S_{ij}]\boldsymbol{\tau}_i\cdot\boldsymbol{\tau}_j, \tag{2.2}$$

$$Y_\pi(r_{ij}) = \frac{e^{-\mu r_{ij}}}{\mu r_{ij}}, \tag{2.3}$$

$$T_\pi(r_{ij}) = \left[1 + \frac{3}{\mu r_{ij}} + \frac{3}{(\mu r_{ij})^2}\right]\frac{e^{-\mu r_{ij}}}{\mu r_{ij}}, \tag{2.4}$$

$$S_{ij} \equiv 3\boldsymbol{\sigma}_i\cdot\hat{\mathbf{r}}_{ij}\boldsymbol{\sigma}_j\cdot\hat{\mathbf{r}}_{ij} - \boldsymbol{\sigma}_i\cdot\boldsymbol{\sigma}_j \tag{2.5}$$

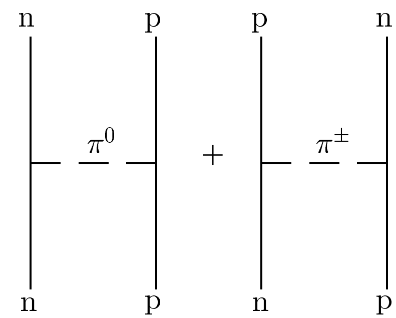

(see HW assignments 8 and 9!)

Argonne (v14-v18)

- One- and 2 pion exchange + phenomenological terms fit to data

$$O^{p}_{ij}=[1,\boldsymbol{\sigma}_i\cdot\boldsymbol{\sigma}_j,S_{ij},(\mathbf{L}\cdot\mathbf{S})_{ij},\mathbf{L}^2_{ij},\mathbf{L}^2_{ij}\boldsymbol{\sigma}_i\cdot\boldsymbol{\sigma}_j,(\mathbf{L}\cdot\mathbf{S})^2_{ij}]$$

$$\otimes[1,\boldsymbol{\tau}_i\cdot\boldsymbol{\tau}_j]. \qquad (2.9)$$

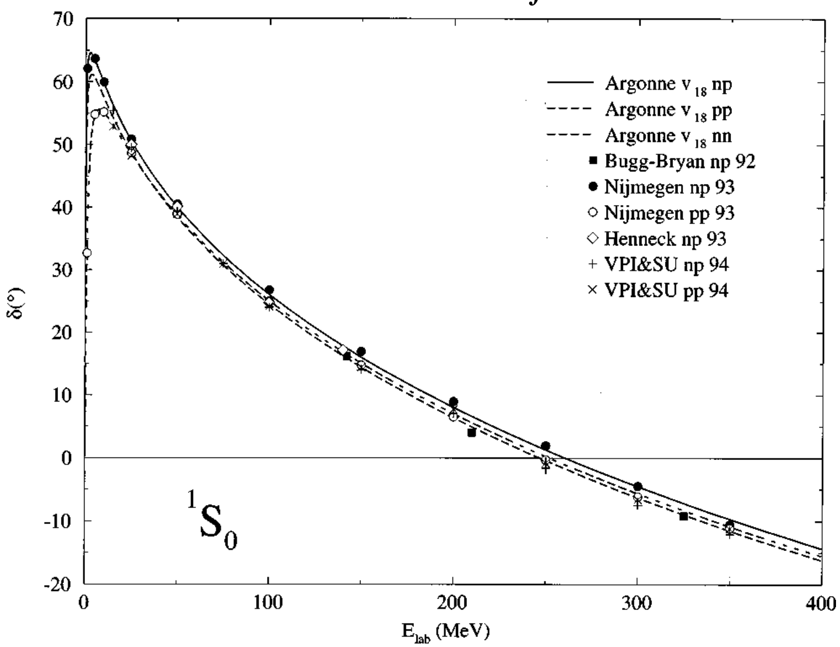

FIG. 3. ${}^1S_0$ phases of the Argonne v_{18} interaction compared to various np and pp phase-shift analyses: Argonne v_{18}, Wiringa, Stoks, and Schiavilla, 1995; Bugg-Bryan, Bugg and Bryan, 1992; Nijmegen, Stoks *et al.*, 1993; Henneck, Henneck, 1993; VPI-SU, Arndt, Workman, and Pavan, 1994. Figure from Wiringa *et al.*, 1995.

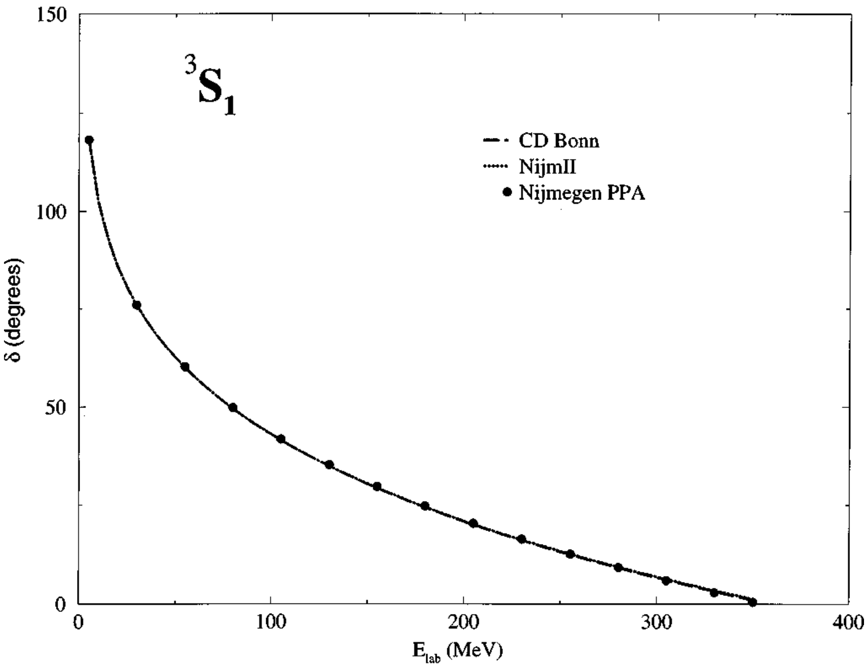

FIG. 5. ${}^3S_1$ phases from different modern NN interaction models: CD Bonn, Machleidt *et al.*, 1996; Nijm II, Stoks, Klomp, *et al.*, 1994; Nijmegan PPA, Stoks, Klomp, *et al.*, 1993. Figure from Wiringa, Stoks, and Schiavilla, 1995.

CD Bonn

Similar Ansatz, but way more mesons (2-meson exchanges) and parameters, but less ad hoc short-range potential -> Can be “naturally” extended to off-shell nucleons.
CD = Charge-dependence; meaning that the slight differences between pn, pp and nn interaction are accounted for.

CD Bonn NN Phase Shifts

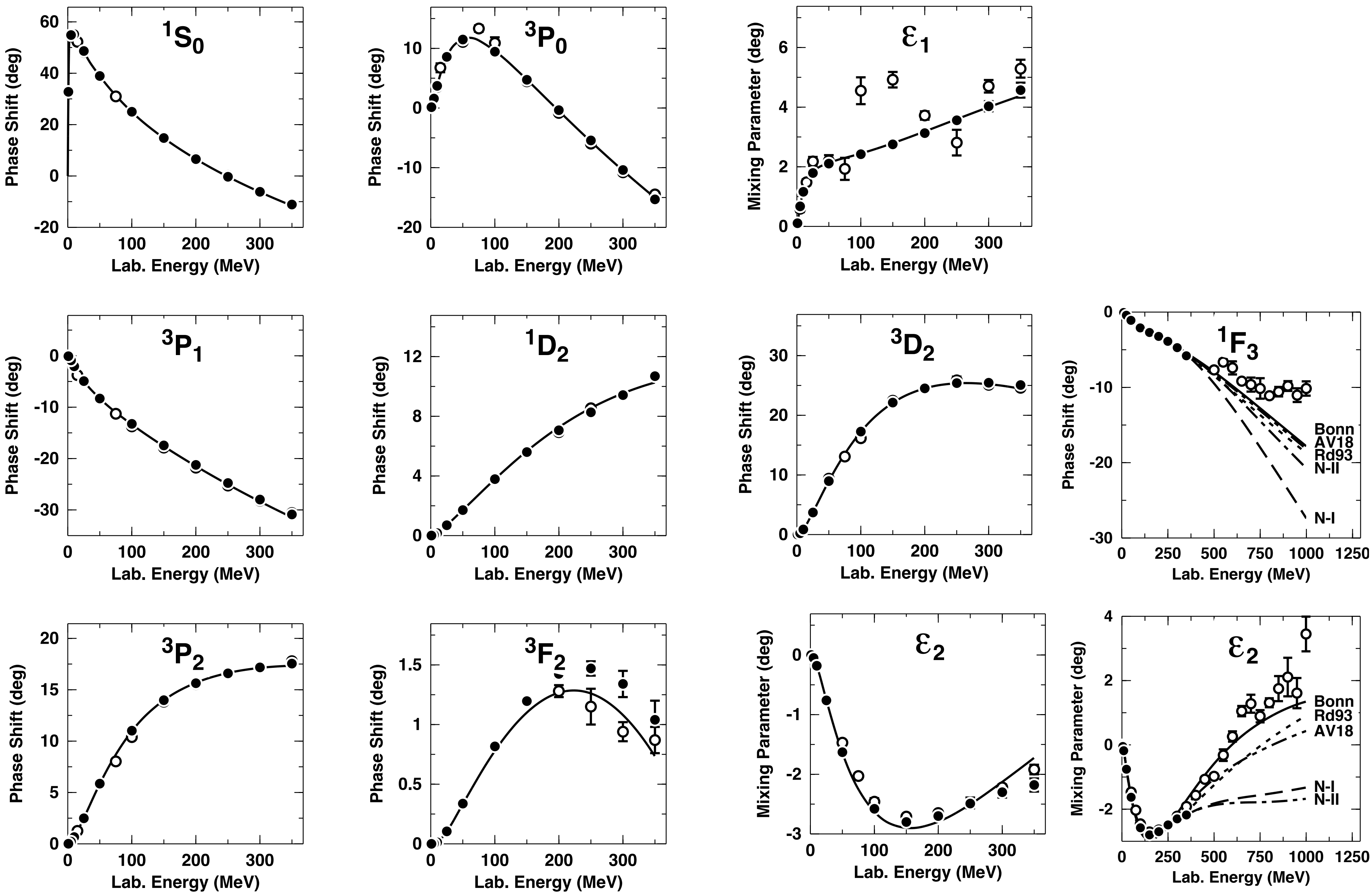

NN forces – the deuteron

Deuteron Properties: Mass = 1865.613 MeV

Only bound NN system

Binding energy 2.225 MeV

$J^P = 1^+$, hence L = 0,2 S = 1, I = 0

RMS radius 1.97 fm (1/2 RMS distance between p and n).

$\mu_D = 0.8574\ \mu_N = \mu_p + \mu_n - 0.0224\ \mu_N$ *)

Electric Quadrupole Moment $Q_D = 0.2859\ e\ \mathrm{fm}^2$ -> some L = 2 admixture!

$P_D = 0.04 - 0.06$ – not an observable! (However, the asymptotic D/S ratio = η is)

TABLE I. Experimental deuteron properties compared to recent *NN* interaction models; meson-exchange effects in μ_d and Q_d are not included.

	Experiment	Argonne v_{18}	Nijm II	Reid 93	CD Bonn	Units
A_S	0.8846(8)[a]	0.8850	0.8845	0.8853	0.8845	$\mathrm{fm}^{1/2}$
η	0.0256(4)[b]	0.0250	0.0252	0.0251	0.0255	
r_d	1.971(5)[c]	1.967	1.9675	1.9686	1.966	fm
μ_d	0.857406(1)[d]	0.847				μ_0
Q_d	0.2859(3)[e]	0.270	0.271	0.270	0.270	fm^2
P_d		5.76	5.64	5.70	4.83	

[a]Ericson and Rosa-Clot, 1983.
[b]Rodning and Knutson, 1990.
[c]Martorell, Sprung, and Zheng, 1995.
[d]Lindgren, 1965.
[e]Bishop and Cheung, 1979.

*) Simple model: $\mu_d = \mu_s - \frac{3}{2}\left(\mu_s - \frac{1}{2}\right) P_D$

NN forces – the deuteron

S- and D-state WF:

$$\psi_M(\mathbf{x}) = \frac{u(r)}{r}\mathcal{Y}^M_{101}(\theta,\phi) + \frac{w(r)}{r}\mathcal{Y}^M_{121}(\theta,\phi)\,, \quad (2)$$

where

$$\mathcal{Y}^M_{JLS}(\theta,\phi) = \sum_{m_L,m_S} \langle J, M\,|L, m_L; S, m_S\rangle\, Y_{LM}(\theta,\phi)\,|S, m_s\rangle \quad (3)$$

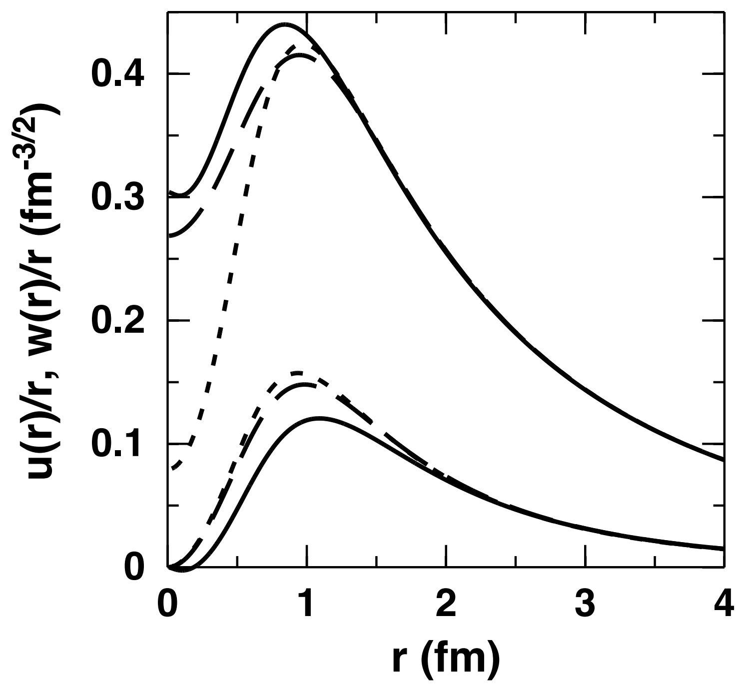

The deuteron wave functions. The family of large curves are u(r)/r and the family of small curves are w(r)/r.

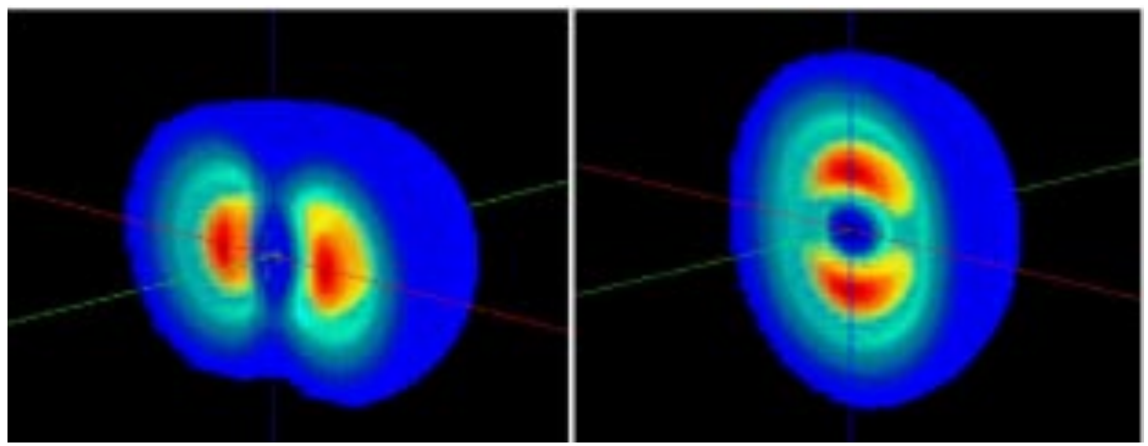

Spatial density contours of the deuteron due to S-D state interference for $S_z = \pm 1$ (left) and $S_z = 0$ (right). z points up.

NN forces – the deuteron

S- and D-state WF:

$$\psi_M(\mathbf{x}) = \frac{u(r)}{r}\mathcal{Y}^M_{101}(\theta,\phi) + \frac{w(r)}{r}\mathcal{Y}^M_{121}(\theta,\phi)\,, \tag{2}$$

where

$$\mathcal{Y}^M_{JLS}(\theta,\phi) = \sum_{m_L,m_S} \langle J,M\,|L,m_L;S,m_S\rangle\, Y_{LM}(\theta,\phi)\,|S,m_s\rangle \tag{3}$$

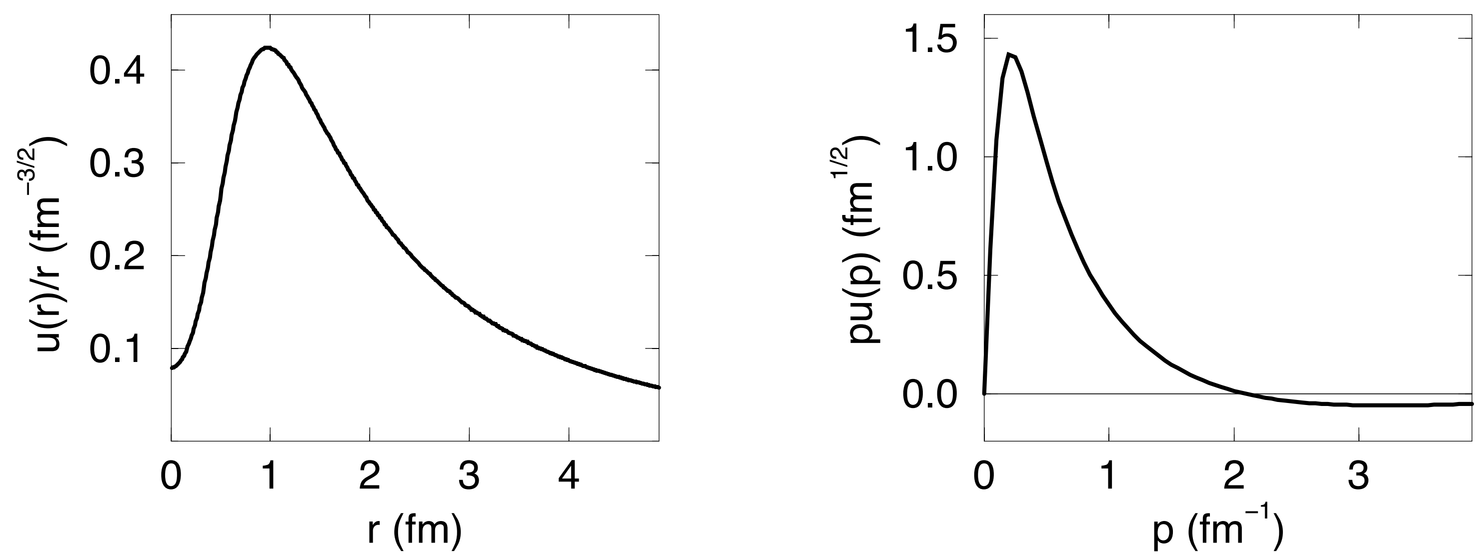

Figure 2: The deuteron S wave function in configuration space and in momentum space: $u(r)/r$ and $pu(p)$ (calculated from the Argonne v_{18} potential).

Deuteron Form Factors

Left: non-relativistic potential model

Right: fully relativistic calculation

Note different horizontal scale (Q vs Q^2, although same maximum)

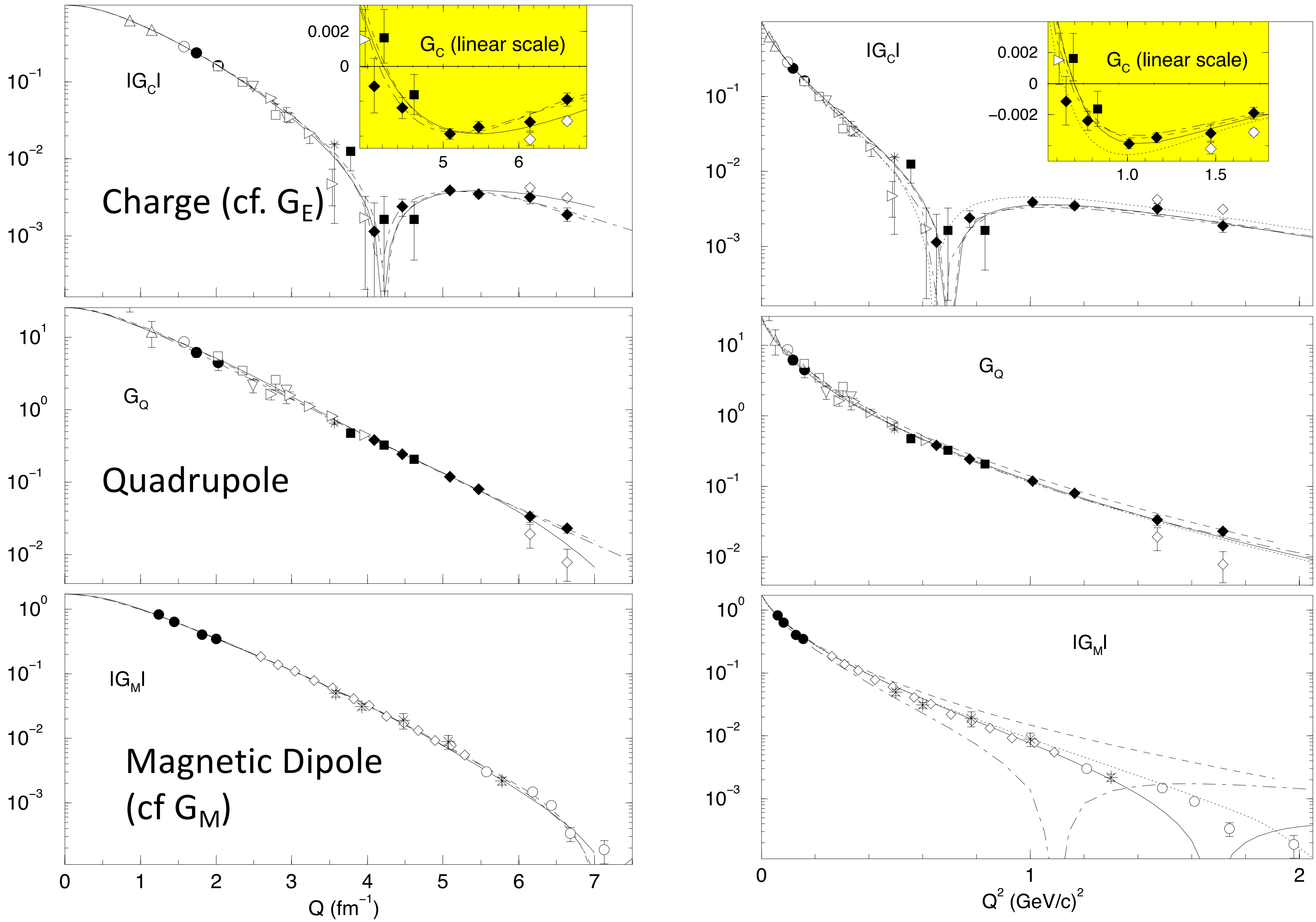

Light Nuclei – from Wikipedia

Tritium, ^{3}H

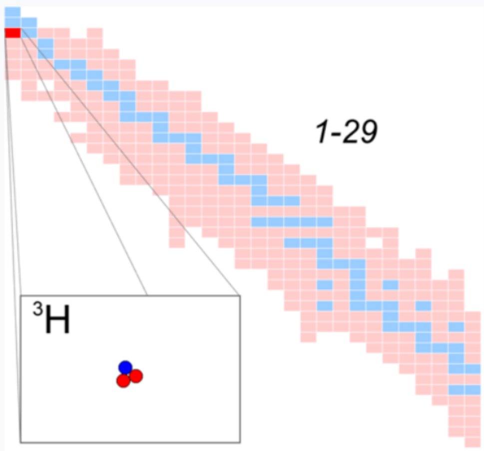

General	
Name, symbol	tritium, ^{3}H
Neutrons	2
Protons	1
Nuclide data	
Natural abundance	trace
Half-life	12.32 years
Decay products	^{3}He
Isotope mass	3.0160492 u
Spin	$\frac{1}{2}$
Excess energy	14,949.794± 0.001 keV
Binding energy	8,481.821± 0.004 keV
Decay modes	
Decay mode	Decay energy (MeV)
Beta emission	0.018590

Complete table of nuclides

Helium-3, ^{3}He

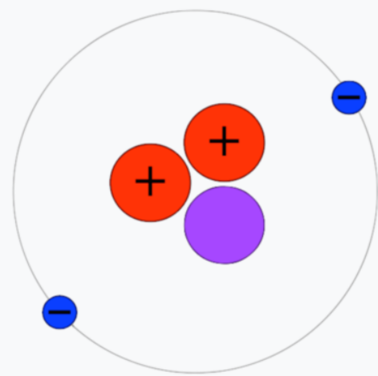

General	
Name, symbol	Helium-3, He-3, ^{3}He
Neutrons	1
Protons	2
Nuclide data	
Natural abundance	0.000137% (% He on Earth)
Half-life	stable
Parent isotopes	^{3}H (beta decay of tritium)
Isotope mass	3.0160293 u
Spin	$\frac{1}{2}$

Note: Isospin doublet
Just like p and n

Helium-4, ^{4}He

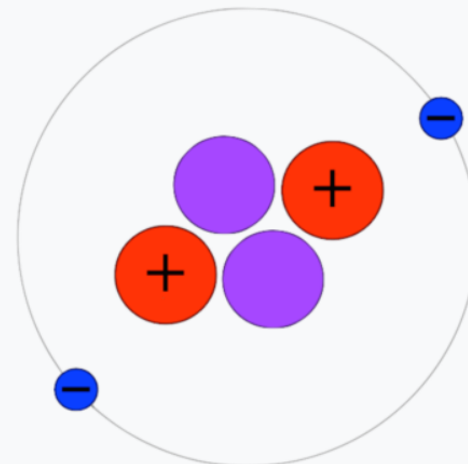

General	
Name, symbol	Helium-4, He-4, ^{4}He
Neutrons	2
Protons	2
Nuclide data	
Natural abundance	99.999863%
Half-life	stable
Isotope mass	4.002602 u
Spin	0
Binding energy	28300.7 keV

Light Nuclei – How to calculate?
(More from Rev. Mod. Phys. 70, 1998)

N-body Hamiltonian $$H=\sum_i \sqrt{\mathbf{p}_i^2+m^2}+\sum_{i<j} v_{ij}(\mathbf{r}_{ij};\mathbf{P}_{ij})$$ NN potential

May have to add 3-body force $$+\sum_{i<j<k} V_{ijk}(\mathbf{r}_{ij},\mathbf{r}_{ik};\mathbf{P}_{ijk}), \qquad (2.12)$$

$$V_{ijk}=V_{ijk}^{2\pi}+V_{ijk}^{R}, \quad V_{ijk}^{R}=U_0\sum_{\mathrm{cyc}} T_\pi^2(r_{ij})T_\pi^2(r_{ik}).$$

arXiv:nucl-th/0102004 1 Feb 2001

Fig. 2 (Pieper, et al.)

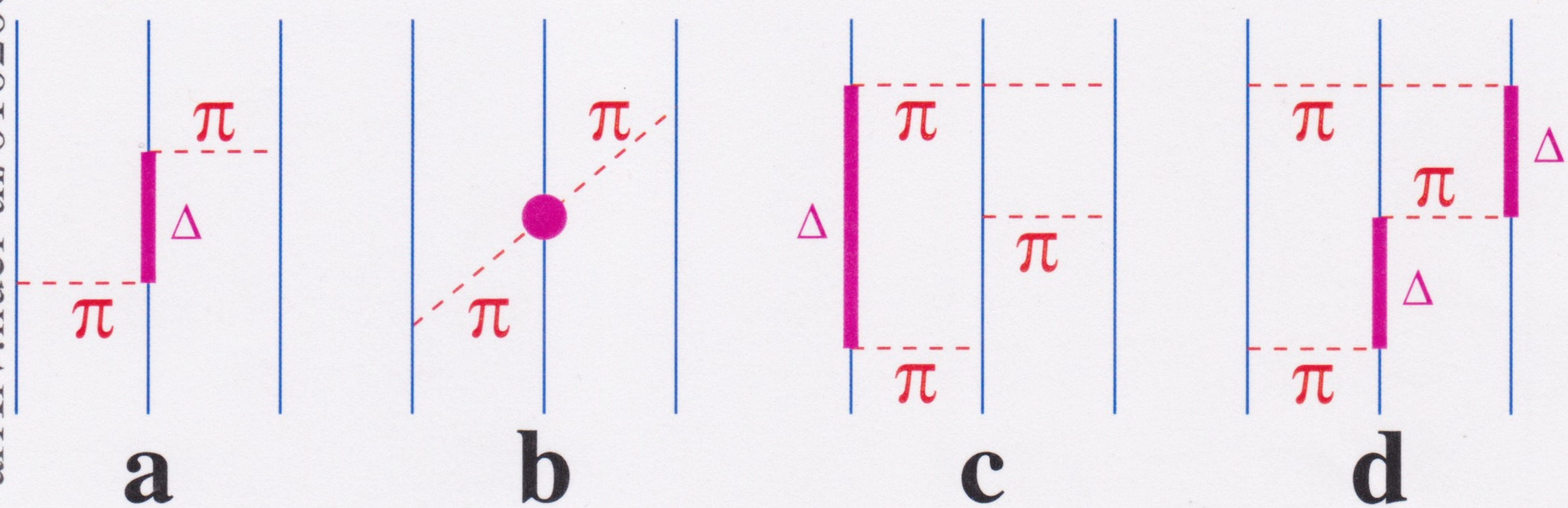

Light Nuclei – how to solve Schrödinger Eq.?

- 3-body -> Fadeev approach: applies to both bound states and scattering. Decomposes 3-body wave function in 3 2-body ones.
- 3-4 body: Hyperspherical harmonics
- ≥3: Monte Carlo methods
  - Variational Monte Carlo (uses variational principle with test functions to find minimum energy = G.S.)
  - Green’s-function Monte Carlo (Path integral, imaginary time,

Light Nuclei

- Some results:

TABLE VI. ^{4}He binding energies with and without three-nucleon interaction; comparison of different methods: correlated hyperspherical harmonics (CHH), Faddeev-Yakubovsky (FY), variational Monte Carlo (VMC), and Green's-function Monte Carlo (GFMC). Error bars in CHH calculations are estimates of the effects of channel truncation.

Hamiltonian	AV14	AV14+TNI 8
CHH	24.17(5)[a]	27.48[b]
FY	24.01[b]	
VMC		27.6(1)[c]
GFMC	24.23(3)[e]	28.3(2)[f]

[a]Viviani, 1997.
[b]Viviani, Kievksy, and Rosati, 1995.
[c]Glöckle *et al.*, 1995.
[d]Arriaga, Pandharipande, and Wiringa, 1995.
[e]Pudliner *et al.*, 1977.
[f]Carlson and Schiavilla, 1994a.

TABLE VII. Experimental and quantum Monte Carlo energies of $A=3-7$ nuclei in MeV (Pudliner *et al.*, 1997), for variational Monte Carlo (VMC), Green's-function Monte Carlo (GFMC), and experiment.

$^AZ(J^\pi;T)$	VMC	GFMC	Expt.
^{2}H$(1^+;0)$	$-2.2248(5)$		-2.2246
^{3}H$(\frac{1}{2}^+;\frac{1}{2})$	$-8.32(1)$	$-8.47(1)$	-8.48
^{4}He$(0^+;0)$	$-27.76(3)$	$-28.30(2)$	-28.30
^{6}He$(0^+;1)$	$-24.87(7)$	$-27.64(14)$	-29.27
^{6}He$(2^+;1)$	$-23.01(7)$	$-25.84(11)$	-27.47
^{6}Li$(1^+;0)$	$-28.09(7)$	$-31.25(11)$	-31.99
^{6}Li$(3^+;0)$	$-25.16(7)$	$-28.53(32)$	-29.80
^{6}Li$(0^+;1)$	$-24.25(7)$	$-27.31(15)$	-28.43
^{6}Li$(2^+;0)$	$-23.86(8)$	$-26.82(35)$	-27.68
^{6}Be$(0^+;1)$	$-22.79(7)$	$-25.52(11)$	-26.92
^{7}He$(\frac{3}{2}^-;\frac{3}{2})$	$-20.43(12)$	$-25.16(16)$	-28.82
^{7}Li$(\frac{3}{2}^-;\frac{1}{2})$	$-32.78(11)$	$-37.44(28)$	-39.24
^{7}Li$(\frac{1}{2}^-;\frac{1}{2})$	$-32.45(11)$	$-36.68(30)$	-38.76
^{7}Li$(\frac{7}{2}^-;\frac{1}{2})$	$-27.30(11)$	$-31.72(30)$	-34.61
^{7}Li$(\frac{5}{2}^-;\frac{1}{2})$	$-26.14(11)$	$-30.88(35)$	-32.56
^{7}Li$(\frac{3}{2}^-;\frac{3}{2})$	$-19.73(12)$	$-24.79(18)$	-28.00

Light Nuclei – more results

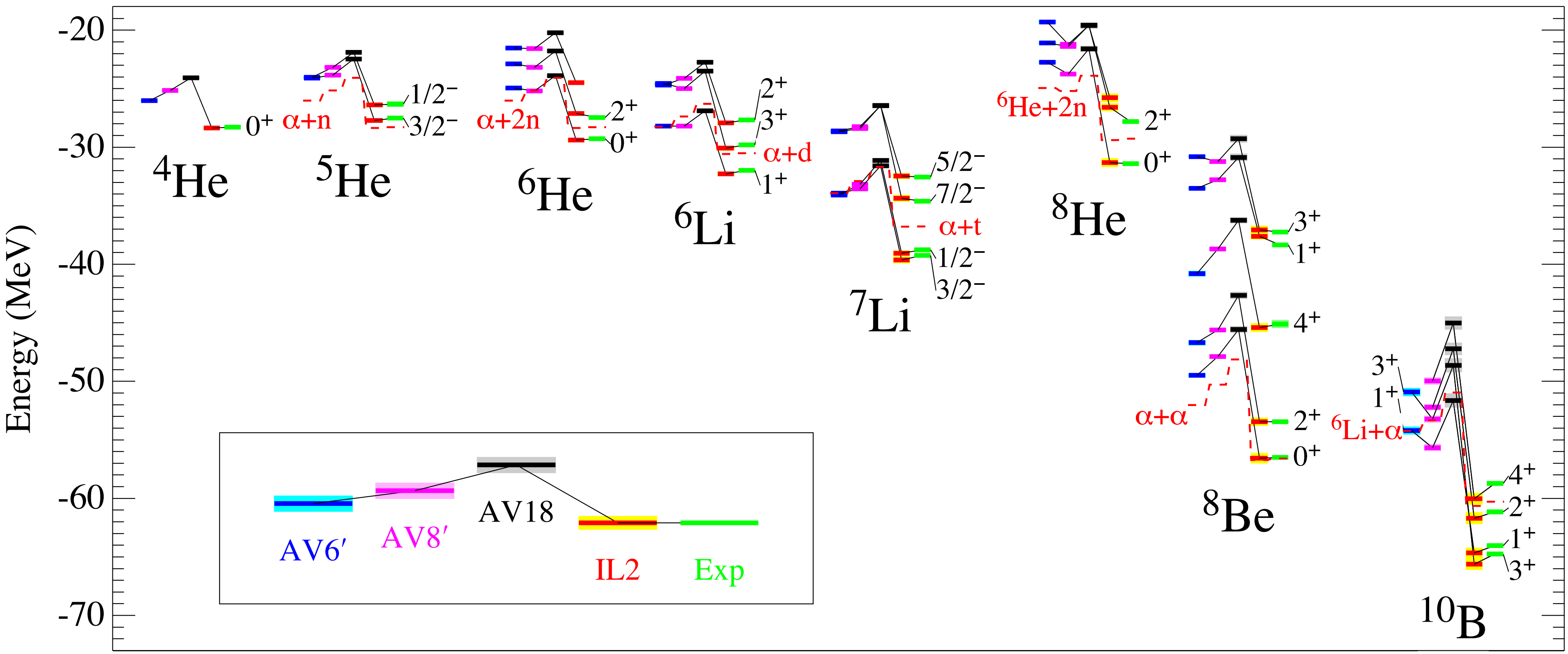

FIG. 2: Nuclear energy levels for the more realistic potential models; shading denotes Monte Carlo statistical errors.

Form Factors of light nuclei

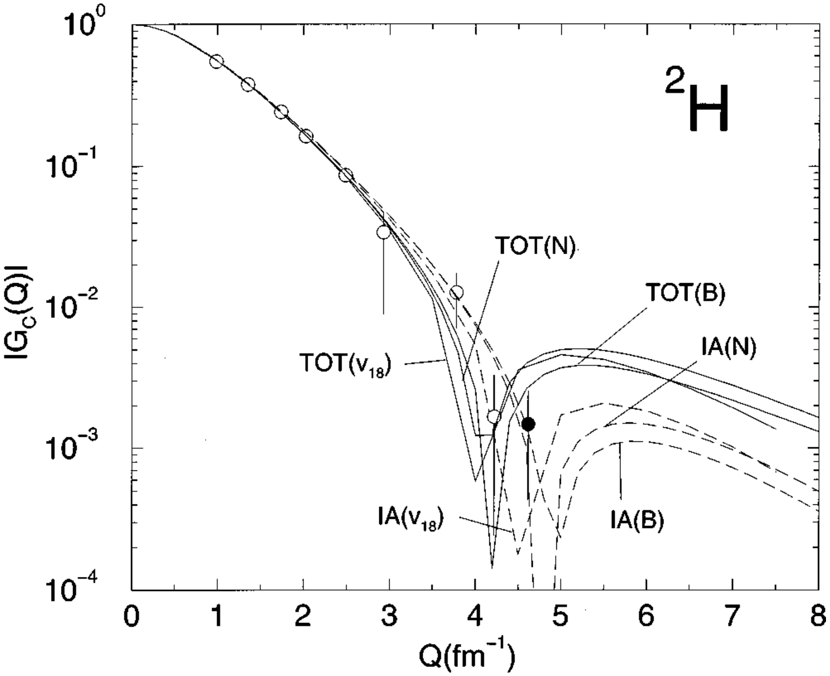

FIG. 18. The charge form factor of the deuteron, obtained in the impulse approximation (IA) and with inclusion of two-body charge contributions and relativistic corrections (TOT), compared with data from Schulze *et al.* (1984), The *et al.* (1991), Dmitriev *et al.* (1985), and Gilman *et al.* (1990) [empty and filled circles denote, respectively, positive and negative experimental values for $G_C(Q)$]. Theoretical results corresponding to the Argonne v_{18} (v_{18}; Wiringa, Stoks, and Schiavilla, 1995), Bonn B (B; Plessas, Christian, and Wagenbrunn, 1995), and Nijmegen (N; Plessas, Christian, and Wagenbrunn, 1995) interactions are displayed. The Höhler parametrization is used for the nucleon electromagnetic form factors.

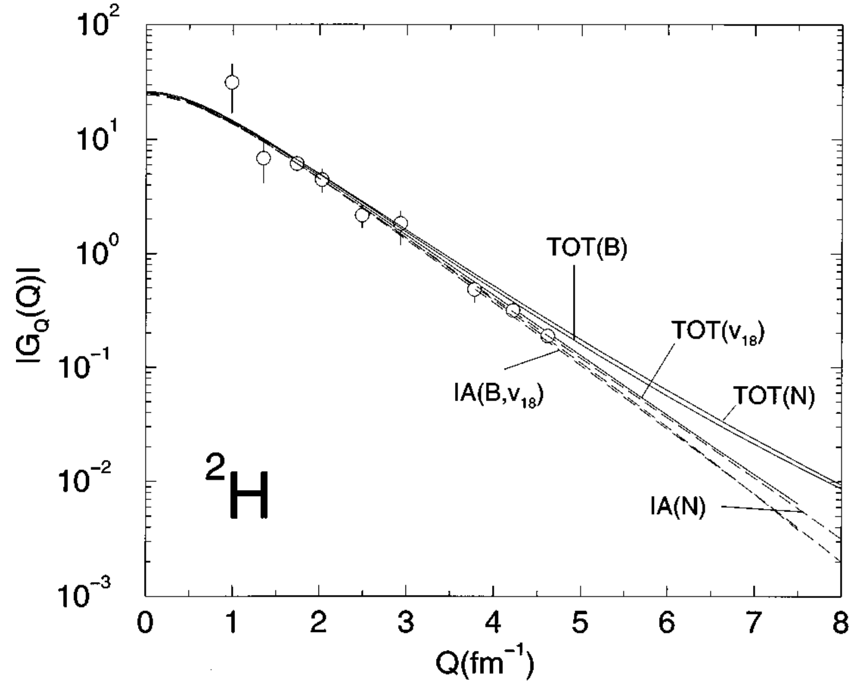

FIG. 19. Same as in Fig. 18, but for the quadrupole form factor of the deuteron.

More light nuclei…

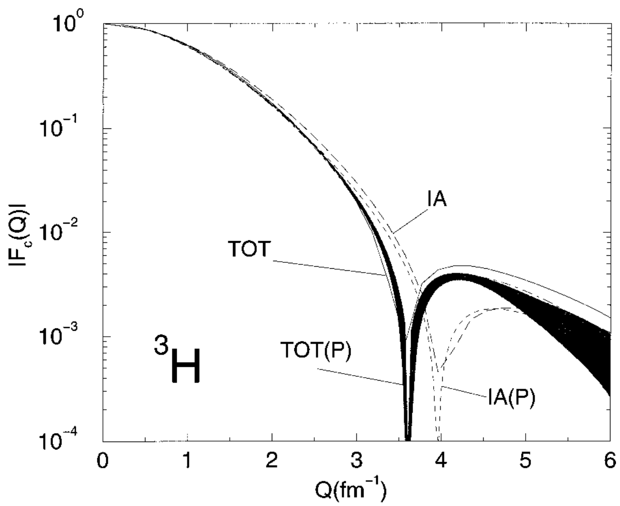

FIG. 27. The charge form factors of ^{3}H, obtained in the impulse approximation (IA) and with inclusion of two-body charge contributions and relativistic corrections (TOT), compared with data (shaded area) from Amround *et al.* (1994).

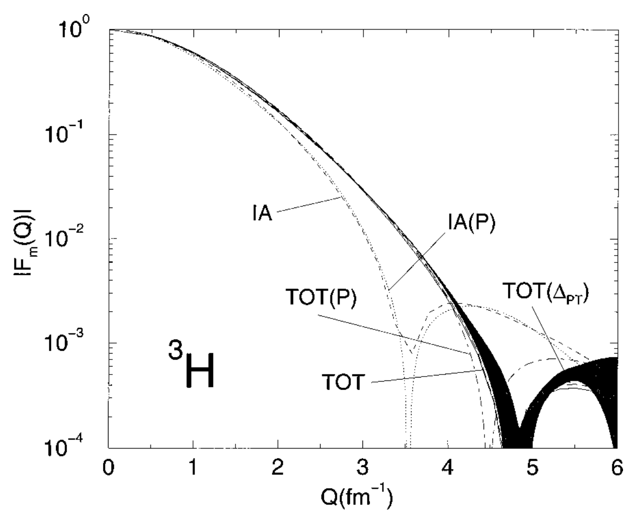

FIG. 25. The magnetic form factors of ^{3}H, obtained in the impulse approximation (IA) and with inclusion of two-body current contributions and Δ admixtures in the bound-state

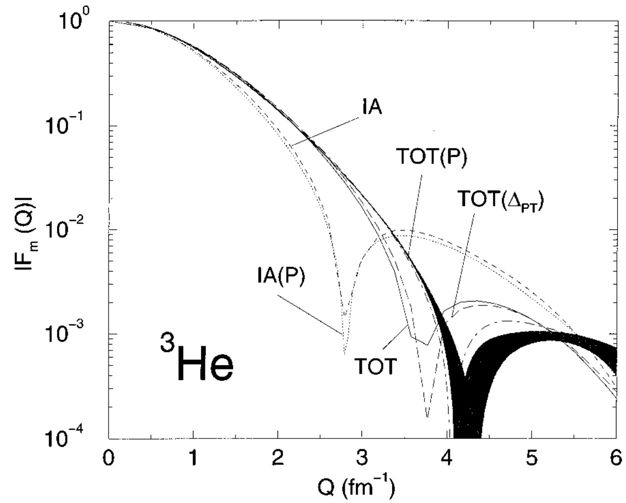

FIG. 26. Same as in Fig. 25, but for ^{3}He.

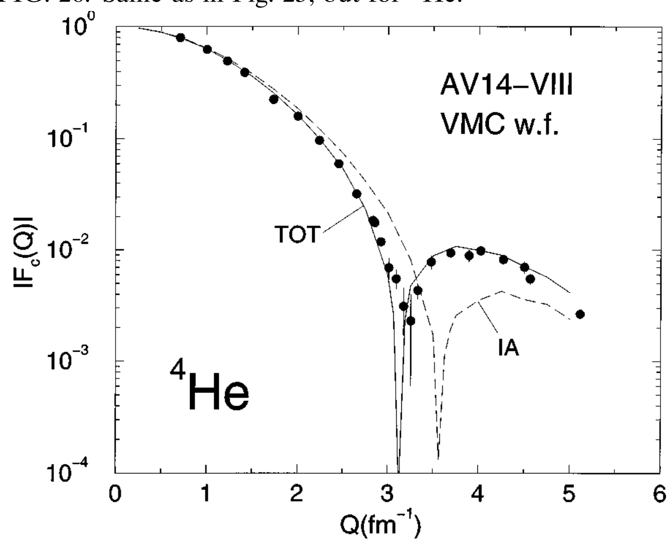

FIG. 29. The charge form factors of ^{4}He, obtained in the impulse approximation (IA) and with inclusion of two-body charge contributions and relativistic corrections (TOT), compared with data from Frosch *et al.* (1968) and Arnold *et al.*

Mixing GFMC wave functions with chiral Effective Field Theory currents:

Magnetic moments in $A \leq 10$ nuclei

Pastore *et al.* (2013)

- GFMC calculations use AV18/IL7 (rather than chiral) potentials with χEFT EM currents
- Predictions for $A > 3$; about 40% of $\mu(^9\text{C})$ due to corrections beyond LO